



This is a repository copy of *Influence of cooling rate on the grain-refining effect of austenite deformation in a HSLA steel.*

White Rose Research Online URL for this paper:
<https://eprints.whiterose.ac.uk/153448/>

Version: Accepted Version

Article:

Zhao, H. and Palmiere, E.J. orcid.org/0000-0002-4048-8536 (2019) Influence of cooling rate on the grain-refining effect of austenite deformation in a HSLA steel. *Materials Characterization*, 158. 109990. ISSN 1044-5803

<https://doi.org/10.1016/j.matchar.2019.109990>

Article available under the terms of the CC-BY-NC-ND licence
(<https://creativecommons.org/licenses/by-nc-nd/4.0/>).

Reuse

This article is distributed under the terms of the Creative Commons Attribution-NonCommercial-NoDerivs (CC BY-NC-ND) licence. This licence only allows you to download this work and share it with others as long as you credit the authors, but you can't change the article in any way or use it commercially. More information and the full terms of the licence here: <https://creativecommons.org/licenses/>

Takedown

If you consider content in White Rose Research Online to be in breach of UK law, please notify us by emailing eprints@whiterose.ac.uk including the URL of the record and the reason for the withdrawal request.



eprints@whiterose.ac.uk
<https://eprints.whiterose.ac.uk/>

Influence of Cooling Rate on the Grain-Refining Effect of Austenite Deformation in a HSLA steel

DOI: <https://doi.org/10.1016/j.matchar.2019.109990>

Haitao Zhao^{a, b*}, Eric J. Palmiere^a

^aThe University of Sheffield, Department of Materials Science and Engineering, Sir Robert Hadfield Building, Mappin Street, Sheffield S1 3JD, UK

^bHBIS Group Technology Research Institute, HBIS Group, Shijiazhuang 050023, China

Corresponding author: H. Zhao, tel: +86 (0)311 6650 8895,

email: zhaohaitao@hbisco.com

Keywords: Austenite deformation; Effective grain size; Acicular ferrite; Bainitic ferrite; cooling rate

Abstract:

Effective grain size is a direct indicator of the high angle grain boundary (HAGB) density of microstructures. A small effective grain size suggests a high density of HAGBs, which provide effective barriers to cleavage fracture. There have been many investigations concerning the effect of processing parameters on the effective grain sizes of steel microstructures. However, contradicting results were found for the influence of austenite deformation. In this research, to understand the influence of austenite deformation on effective grain size refinement, a low carbon Nb microalloyed steel was subjected to different austenite deformation conditions and was continuously cooled at a wide range of cooling rates (0.5~50°C/s). Characteristics of transformed microstructures from recrystallised and deformed austenite were

analysed through optical microscopy observation and EBSD mapping. In the whole cooling rate range adopted in this research, effective grain sizes were found to be refined by austenite deformation. However, with the rise of cooling rate higher than 10°C/s . With the rise of the cooling rate higher than 10°C/s , effective grain sizes are reduced for recrystallised austenite, while increasingly large effective grain sizes were found for deformed austenite. According to these experimental results, the influence of austenite deformation on effective grain size in a wider cooling rate range was proposed to be cooling rate dependent, and possible explanations for the contradicting results in the literature were discussed based on that.

1 Introduction

It is well acknowledged that high angle grain boundaries (HAGBs), which have misorientation angles greater than 15° , are one of the factors affecting a steel's toughness. A high density of HAGBs provide effective barriers to cleavage fracture by arresting cleavage cracks or deviating their propagation directions [1, 2]. Increasing the HAGBs density of steel microstructures could enhance their toughness [3]. The average size of grains surrounded by HAGBs, which is usually called the effective grain size, is a very important microstructural parameter because it is an indicator of the density of HAGBs [4, 5].

There have been many investigations concerning the effect of processing parameters on the effective grain sizes of steel microstructures [6-11]. However, some of the results are still controversial, especially for the influence of austenite deformation below the austenite nil-recrystallisation temperature (T_{nr}). Austenite deformation below T_{nr} is the essence of thermomechanical processing [12]. After deformation, several changes in the austenite state are made, including grain shape, texture, substructure density, annealing twin boundaries and bulging of austenite grain boundaries [13]. This austenite conditioning strongly affects the transformed microstructures [14, 15].

For Nb microalloyed steels, Beynon and Sellars [16] found that the mean grain

size of ferrite is reduced by austenite deformation. In our previous investigation [10] for a low carbon Nb microalloyed steel cooled at 20°C/s, the effective grain size is decreased from 5.7 μm to 3.1 μm with the austenite strain rising from 0 to 0.5. In research [17], on a low carbon Nb-V microalloyed steel, it was found that the effective grain size of microstructures transformed from deformed austenite is smaller than those of microstructures transformed from recrystallised austenite in a wide cooling rate range (0.2~30°C/s), and this grain-refining effect of austenite deformation gradually becomes weak as the cooling rate increases.

Contradicting these are the results found in the literature that austenite deformation leads to microstructure coarsening [11, 18-20]. It was shown that for a low carbon vanadium microalloyed Ni-Cu-Mo-Cr steel with an austenite grain size of 47 μm, the effective grain size of bainite was increased from 3.2 μm to 3.8 μm when austenite was deformed by 30% and cooled at 50°C/s [11]. For a low carbon vanadium microalloyed steel with a larger austenite grain size of 140 μm, the effective grain size was also increased from 5.1 μm to 5.3 μm when austenite was deformed by 30% and cooled at 50°C/s [18]. The block width of bainite transformed at 350 °C was found to be increased after an austenite deformation of 50% for Fe-9Ni-C alloys with carbon contents of 0.3 and 0.5 wt.%, respectively [19]. For a TRIP steel with 0.4 wt.% C, 1.5 wt.% Si and 1.5 wt% Mn, the quantity of bainite packets transformed at 400 °C in each austenite grain was found decreased after austenite deformation [20].

Given these contradicting results found in the literature, the influence of austenite deformation on the effective grain size of transformed microstructures was investigated in a wide cooling rate range for a low carbon Nb microalloyed steel. Explanations for different grain-refining effects of austenite deformation are provided in respect of the transformed microstructure's characteristics.

2 Experimental

The chemical composition of the steel used is shown in Table 1. In order to fully dissolve the Nb-containing precipitates and shorten the preheating time during testing,

all specimens were subjected to a solid-solution heat treatment at 1250°C for 30 minutes with argon atmosphere protection, and were water quenched directly from 1250°C to room temperature.

Table 1 Chemical Compositions (wt%)

C	Mn	Si	S	P	Nb	Cr	Ni	Cu	Ti	N
0.045	1.43	0.14	<0.003	<0.01	0.09	0.21	0.12	0.21	0.01	0.0039

Plane strain compression and subsequent controlled cooling tests were carried out on the servo-hydraulic thermomechanical compression (TMC) machine at The University of Sheffield. The processing route is schematically illustrated in Figure 1. The solid solution heat treated specimens were reheated to 1200°C at a rate of 10°C/s, held 2 minutes for equilibration, and then cooled at a rate of 5°C/s to 1100°C for a roughing deformation (strain1) of 0.3 at a constant true strain rate of 10s⁻¹. After the roughing deformation, the specimens were cooled immediately to 950°C at a rate of 5°C/s for the second deformation with strain2 of either 0 or 0.5. As the typical T_{nr} for HSLA steels containing 0.1 wt% niobium is close to 1050°C [19], the second deformation temperature was selected as 950°C. This second deformation was also performed at a constant true strain rate of 10s⁻¹, and was followed by a controlled cooling from 950°C to 500°C at rates of 0.5°C/s, 1°C/s, 5°C/s, 10°C/s, 20°C/s and 50°C/s, respectively. After that, specimens were slowly cooled from 500°C to 350°C at a rate of 1°C/s, and finally were water quenched from 350°C to room temperature. Going through the same processing route, another two samples were water quenched directly after strain2 of 0 and 0.5, respectively, to examine the austenite morphology.

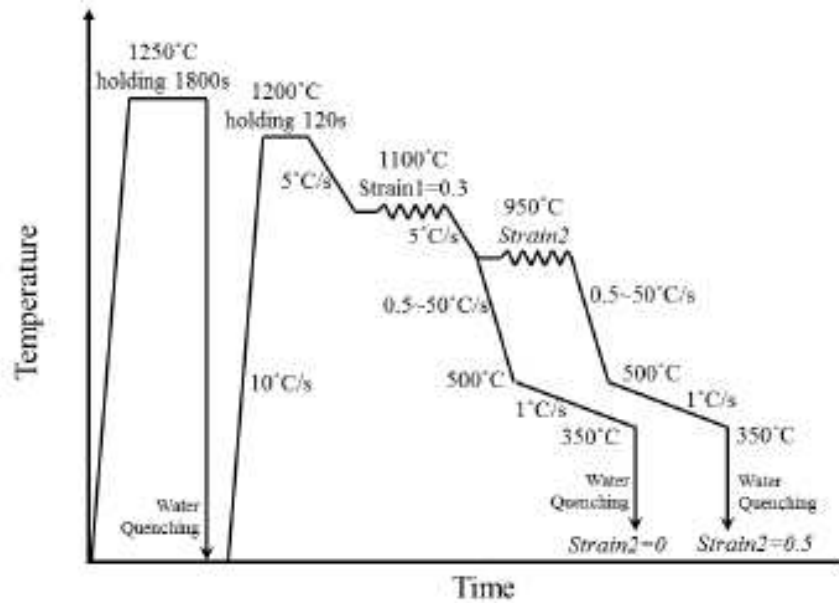


Figure 1 Schematic illustration of the thermomechanical testing profile.

Samples for metallographic observation were cut in the rolling direction (RD)–normal direction (ND) plane and polished. A 2% nital solution was used to show the transformed microstructure and a saturated aqueous picric acid solution was used to reveal the prior-austenite grain boundaries (PAGBs). The prior-austenite grain size was measured optically by the linear intercept method. Optical microscopy (OM) observations were carried out on a Nikon Eclipse LV150.

To prepare specimens particularly for EBSD mapping, after grinding and polishing the specimens were then polished further with a colloidal silica suspension for additional 2 minutes. EBSD mappings were performed on a FEI Sirion electron microscope with a HKL Nordlys detector. Orientation maps with an accelerating voltage of 20kV were obtained on the RD-ND plane for each sample. The step size for the transformed microstructures with cooling rates of 0.5°C/s and 1°C/s was set at 0.5 μm because coarse PF/QF grains dominate these transformed microstructures. The step size for the rest of the cooling rates was set at 0.2 μm . To reduce the mis-indexing of phases in these complex microstructures, α iron (BCC) was chosen as the only matching unit. Following a recommended method [38], noise points of raw data were removed and non-indexed points were filled with the common orientation of their neighbours using HKL Channel 5 Tango software.

3 Results

3.1 Prior-austenite microstructures

Micrographs of the prior-austenite grains with strain2 of 0 and 0.5 are shown in Figure 2 a~b, respectively. As can be seen from these two figures, with strain2 of 0, the prior-austenite grains are recrystallised and the mean linear intercept length measured grain size is 37.0 μm , while with a strain2 of 0.5, the prior-austenite microstructure remains in a deformed condition. Based on that, the selected austenite deformation parameters are considered suitable to investigate the effect of austenite deformation on the effective grain size of transformed microstructures.

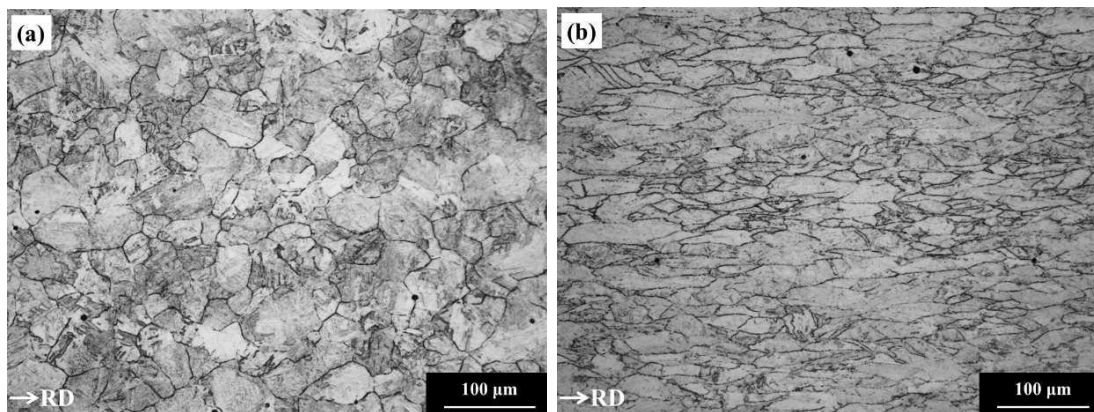


Figure 2 Optical micrographs depicting prior austenite grain boundaries of water quenched sample from 950°C: (a) after strain2=0 and (b) after strain2=0.5.

3.2 Transformed microstructures

During the continuous cooling of HSLA steels, various transformation products can be formed and specific terms have been introduced to describe these products. The classification of ferritic microstructures proposed by Araki et al. [21] and Krauss et al. [22] was used in this research, including polygonal ferrite (PF), quasi-polygonal ferrite (QF), granular bainite (GB), acicular ferrite (AF) and lath bainite (LB).

PF and QF are reconstructive transformation products. PF forms at the slowest cooling rates and the highest transformation temperatures. It nucleates at austenite grain boundaries and grows into an equiaxed shape [22]. QF often forms in very-low-carbon steels under rapid cooling. In this condition, single-phase austenite can transform into single-phase ferrite without a composition change, and the QF grains formed by massive transformation are usually coarse and have irregular and jagged grain boundaries [23].

At low transformation temperatures, AF, GB and LB transformations become dominant [24, 25]. AF was defined by Smith et al. [26] in 1972 as “a highly substructured, non-equiaxed ferrite that forms upon continuous cooling by a mixed diffusion and shear mode of transformation that begins at a temperature slightly higher than the upper bainite transformation range”. It has distinct morphology characteristics like small grain sizes, irregular grain shapes and a chaotic grain arrangement [26-28]. GB is usually formed at relatively higher temperatures and mainly consist of wide parallel laths [7]. It is difficult to observe these lath boundaries and only its packet boundaries can be revealed clearly [9], which makes GB packets looks like grains with an almost entirely granular aspect [10]. Differently, LB packets form at relatively lower temperatures and consist of fine parallel laths [11]. As these lath boundaries can be shown clearly after etching, LB has a clear lath-like morphology [9]. Despite the difference in morphology, GB is not different from LB in terms of the transformation mechanism, and both of them mainly consist of parallel laths and contain a high density of dislocations [10]. Therefore, in this research, both GB and LB are termed as bainitic ferrite (BF). Microstructures transformed from the *recrystallised* austenite (strain2=0) with different cooling rates are shown in Figure 3.

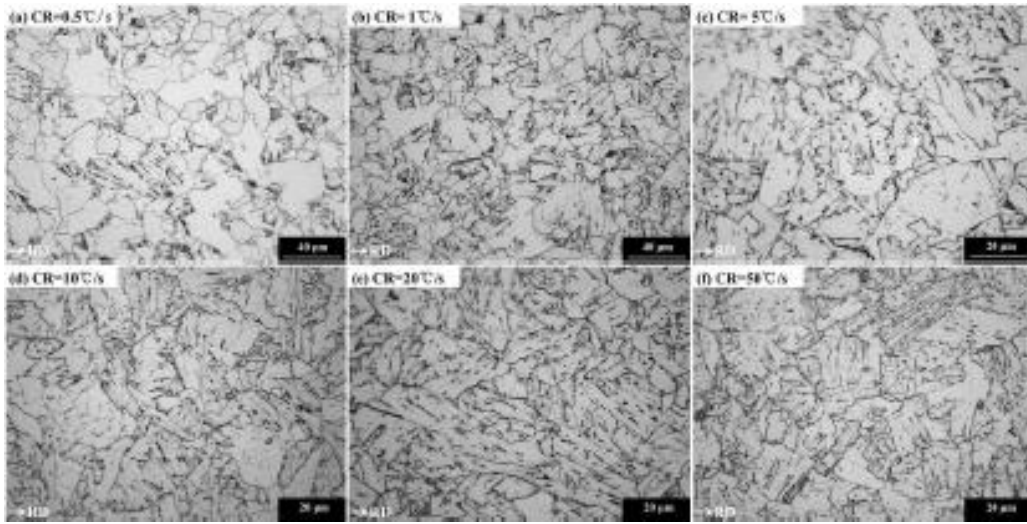


Figure 3 Optical micrographs depicting microstructures transformed from recrystallised austenite (strain₂=0) with different continuous cooling rates: (a) 0.5°C/s, (b) 1°C/s, (c) 5°C/s, (d) 10°C/s, (e) 20°C/s and (f) 50°C/s.

At cooling rates of 0.5°C/s and 1°C/s, Figure 3a~b, a mixture of PF/QF grains and BF packets was found in the transformed microstructures, and with the increase of cooling rates, the volume fraction of BF rises and the grain size of PF/QF becomes smaller.

At cooling rates higher than 1°C/s, Figure 3c~f, a parallel morphology of the transformed products can be seen clearly in all microstructures. PAGBs remain, and the parallel laths developed from the PAGBs extended into the austenite grains, sometimes across the whole grain, which is a typical BF morphology. Therefore, BF dominates the transformed microstructures continuously cooled at 5~50°C/s without austenite deformation. At the cooling rate of 5°C/s (Figure 3c), the microstructure mainly consists of coarse BF laths and some of the lath boundaries can only be seen vaguely. Differently, at the cooling rate of 50°C/s (Figure 3f), BF laths become thinner and the lath boundaries are clearer. With the increase of cooling rate from 5°C/s to 50°C/s, the transformed microstructure gradually changes from coarse BF laths to thin BF laths, and the boundaries between laths are increasingly clear.

Microstructures transformed from *deformed* austenite (strain₂=0.5) with different

cooling rates are shown in Figure 4. At cooling rates of 0.5°C/s and 1°C/s (Figure 4a~b), a mixture of PF/QF grains and dark phases was found, and increasing the cooling rate, the grain size of PF/QF becomes smaller. The phases appearing dark in the optical micrographs could be conventional bainite with carbides or degenerated pearlite, and a detailed TEM observation of thin foils is required to give a definite answer, which is outside the scope of this study. In contrast to the microstructures transformed from *recrystallised* austenite, under these low cooling rates, parallel BF laths no longer exist in the microstructures transformed from *deformed* austenite.

With cooling rates between 5~20°C/s (Figure 4c~e), the transformed microstructures mainly consist of AF laths, together with a small fraction of PF/QF grains at the lower cooling rate (5°C/s) or parallel BF laths at the higher cooling rates (10~20°C/s). Increasing the cooling rate further to 50°C/s, a parallel morphology of the transformed product becomes evident and many laths developed across the entire austenite grains, which is a typical BF dominant microstructure.

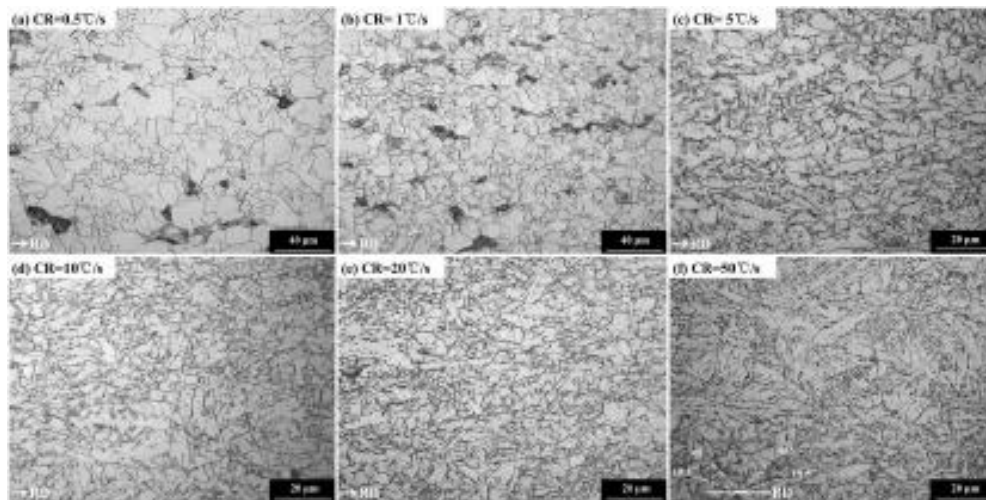


Figure 4 Optical micrographs depicting microstructures transformed from deformed austenite (strain₂=0.5) with different continuous cooling rates from 950°C to 500°C: (a) 0.5°C/s, (b) 1°C/s, (c) 5°C/s, (d) 10°C/s, (e) 20°C/s and (f) 50°C/s.

3.3 EBSD Mappings

Following the noise reduction procedures illustrated in reference [38], a small area of each EBSD data set was used to plot an inverse pole figure (IPF) coloured orientation map and a boundary map. For the statistical analysis of the boundary intercept length, the entire data set was used.

The selected area IPF coloured orientation maps and corresponding boundary maps of the microstructures transformed from *recrystallised* and *deformed* austenite with different cooling rates are shown in Figures 5 and 6, respectively.

If transformed from *recrystallised* austenite, increasing the cooling rate from 0.5°C/s to 1°C/s (Figure 5a~b and Figure 5g~h), the grain size of PF/QF decreases and the area fraction of BF with a high density of low angle grain boundaries (LAGBs) rises, which corresponds very well with the optical micrographs (Figure 3). With the cooling rate increasing from 5°C/s to 20°C/s (Figure 5c~e), the change in the effective grain size is not evident. It can be seen that these transformed microstructures mainly consist of coarse BF packets, and HAGBs mainly exist between packets instead of between laths within packets. Furthermore, from the corresponding boundary maps (Figure 5i~k), it can be found that within each packet LAGBs were generated and the influence of cooling rate on the densities of both HAGB and LAGB is not evident. However, increasing the cooling rate further to 50°C/s , the densities of both HAGB and LAGB are increased significantly and HAGBs exist not only between packets but also between laths within packets, forming straight and parallel HAGBs in Figure 5l.

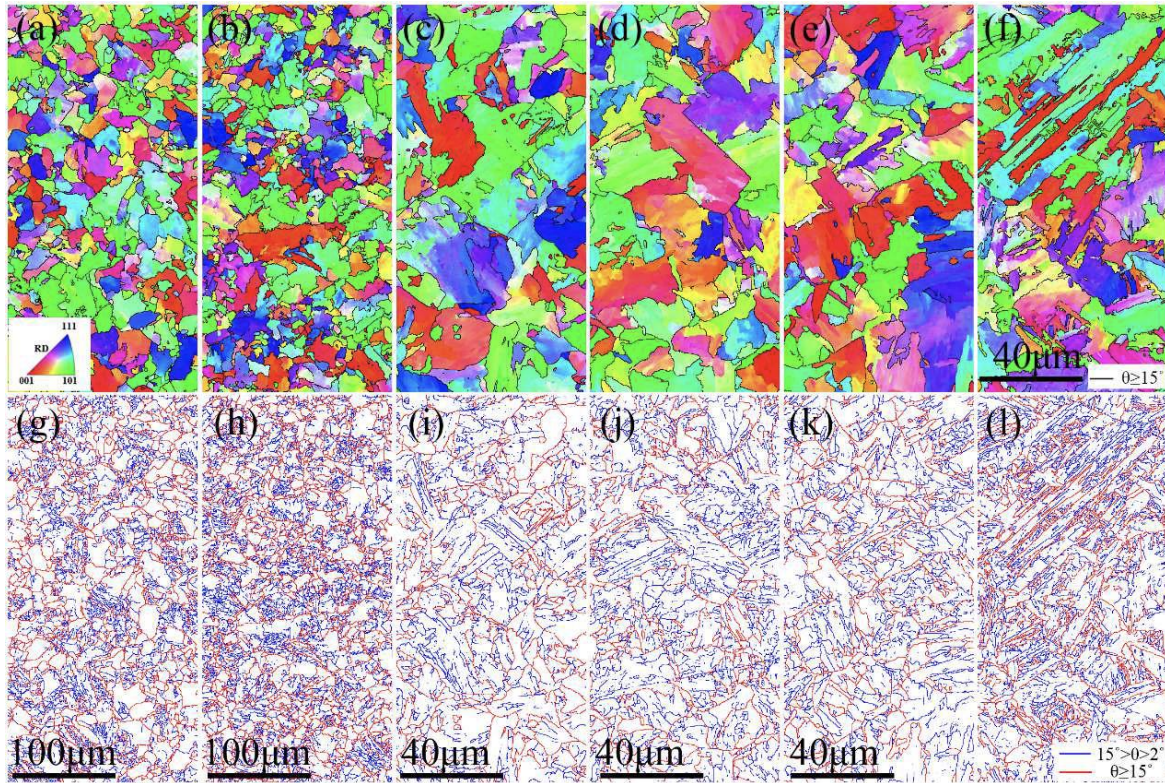


Figure 5 EBSD maps of the microstructures transformed from *recrystallised* austenite (strain₂=0) with different continuous cooling rates from 950°C to 500°C: (a~f) inversepole figure coloured orientation maps corresponding to microstructures with cooling rates of 0.5°C/s, 1°C/s, 5°C/s, 10°C/s, 20°C/s and 50°C/s respectively, where black lines represent high angle boundaries with misorientation angles greater than 15°; (g~l) boundary maps corresponding to the same area in (a~f) respectively, where blue lines represent low angle boundaries with misorientation angles between 2° and 15° whilst red lines represent high angle boundaries with misorientation angles greater than 15°.

If transformed from *deformed* austenite, increasing the cooling rate from 0.5°C/s to 1°C/s (Figure 6a~b), the grain size of PF/QF decreases. With the cooling rate rising from 5°C/s to 10°C/s (Figure 6c~d), the density of HAGBs is increased because the relatively coarse PF/QF grains in Figure 6c are replaced by the fine AF laths in Figure 6d. But raising the cooling rate from 10°C/s to 50°C/s, the area of coarse effective grains increases and finally leads to a quite inhomogeneous microstructure at the cooling rate of 50°C/s. Meanwhile, the density of LAGBs increases constantly with the cooling rate rising from 5°C/s to 50°C/s as shown in Figure 6i~l.

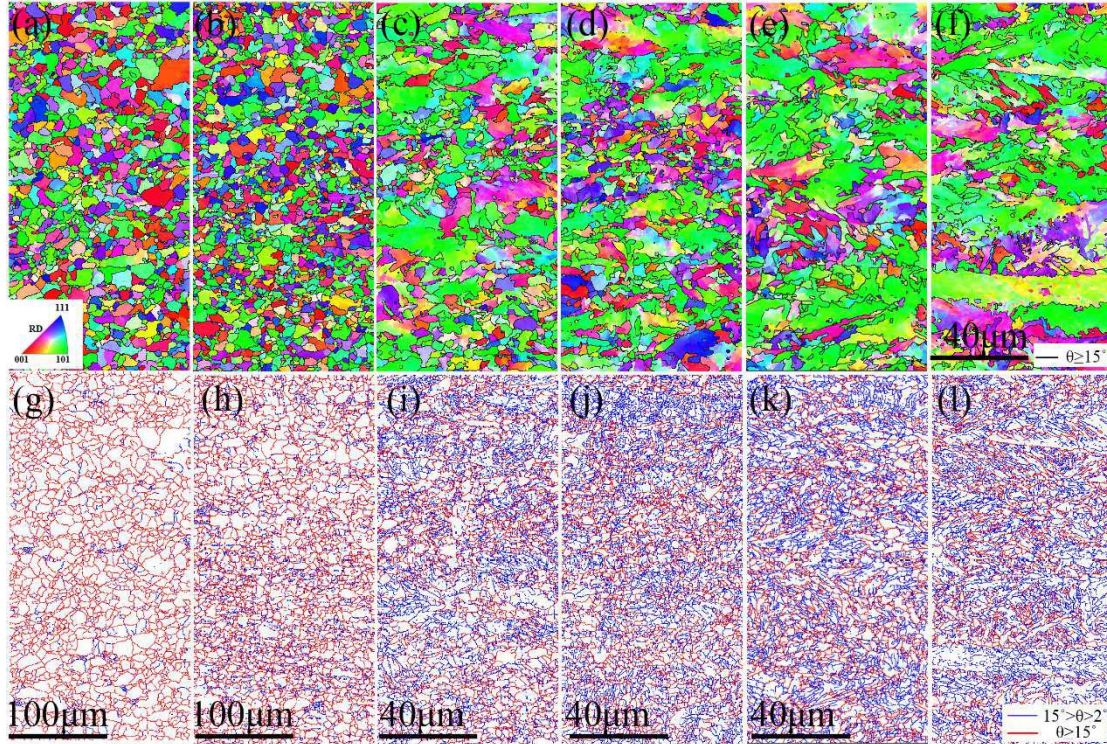


Figure 6 EBSD maps of the microstructures transformed from deformed austenite (strain₂=0.5) with different continuous cooling rates from 950°C to 500°C: (a~f) inverse pole figure coloured orientation maps corresponding to microstructures with cooling rates of 0.5°C/s, 1°C/s, 5°C/s, 10°C/s, 20°C/s and 50°C/s respectively, where black lines represent high angle boundaries with misorientation angles greater than 15°; (g~l) boundary maps corresponding to the same area in (a~f) respectively, where blue lines represent low angle boundaries with misorientation angles between 2° and 15° whilst red lines represent high angle boundaries with misorientation angles greater than 15°.

To quantify the microstructure's refinement, misorientation angle threshold values should be selected. Misorientation angles of 4° and 15° are typical threshold values to define the microstructural unit sizes responsible for strengthening and toughening,

respectively [4, 5]. Grain sizes defined by different misorientation threshold values of 4° and 15° , respectively, were measured by a linear intercept method with the Channel 5 software. The geometric means of the linear intercept lengths in both horizontal and vertical directions were calculated as in reference [38] and are shown in Figure 7.

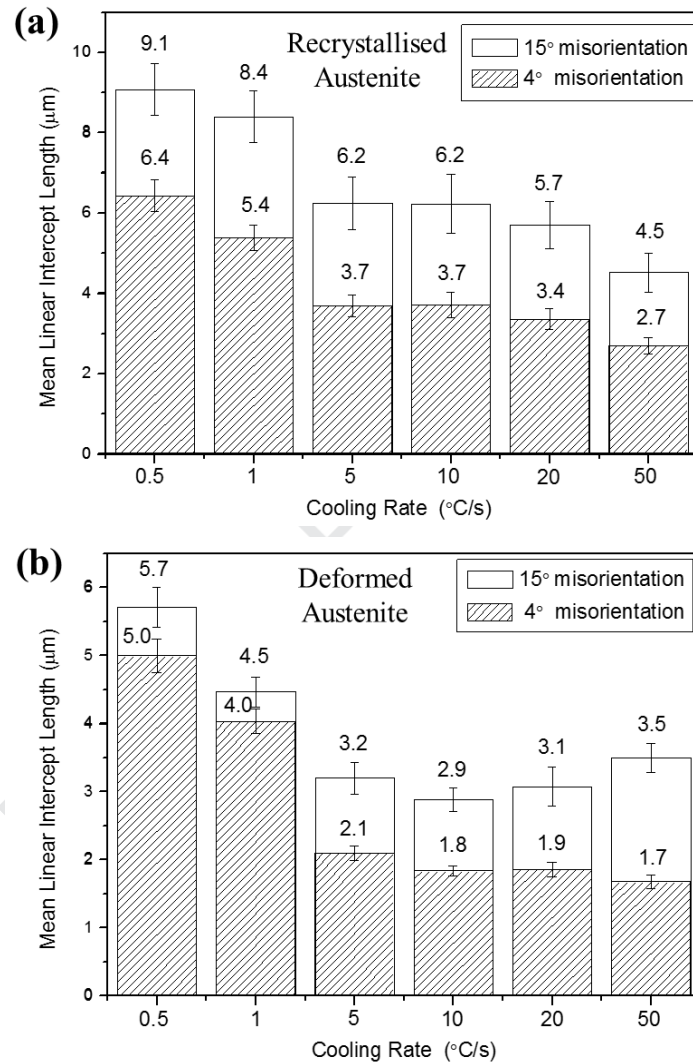


Figure 7 Microstructure size parameters measured as the geometric mean of the linear interception lengths in horizontal and vertical directions from the EBSD maps of the microstructures transformed from (a) recrystallised austenite and (b) deformed austenite, where error bars represent 95% confidence levels of the measurement.

For transformed microstructures from *recrystallised* austenite, the grain sizes

defined by both misorientation threshold values of 4° and 15° , are reduced with the cooling rate increasing from 0.5°C/s to 50°C/s . The changes of grain size between cooling rates of 5°C/s to 20°C/s , however, are not statistically significant as there are very large overlaps of their 95% CL error bars, but they correspond very well with the results obtained from EBSD maps in Figure 5.

Differently, for microstructures transformed from *deformed* austenite, the change of grain size with cooling rate is more complicated. For the grain size defined by the misorientation threshold value of 4° , the grain size is firstly reduced from $5.0\ \mu\text{m}$ to $1.8\ \mu\text{m}$ with the cooling rate increasing from 0.5°C/s to 10°C/s , and then the grain size is raised to $1.9\ \mu\text{m}$ although this increase is not statistically significant. Finally, when the cooling rate reaches 50°C/s , the grain size is further lowered to $1.7\ \mu\text{m}$. While for the grain size defined by the misorientation threshold value of 15° , the effective grain size firstly is reduced from $5.7\ \mu\text{m}$ to $2.9\ \mu\text{m}$ with the cooling rate increasing from 0.5°C/s to 10°C/s , and then the effective grain size is increased continuously from $2.9\ \mu\text{m}$ to $3.5\ \mu\text{m}$ as the cooling rate is raised from 10°C/s to 50°C/s , although the effective grain size change between 10°C/s and 20°C/s is not statistically significant.

4 Discussion

4.1 Transformed microstructures at slow cooling rates

4.1.1 Transformed from recrystallised austenite

Without austenite deformation, the transformed microstructures cooled at 0.5°C/s and 1°C/s consist of PF/QF grains and BF packets. The appearance of the BF packets can be attributed to the effect of niobium on the steel's hardenability. It has been found by many researchers [29-31] that the addition of niobium in solution can suppress the allotriomorphic ferrite transformation by lowering its nucleation rate at austenite grain boundaries and promote bainitic transformation microstructures. In microalloyed steels, the concentration of niobium is normally lower than 0.1% [32]. This indicates that the effect of niobium on the steel's hardenability should be very

limited. However, niobium atoms in solution do not evenly distribute in austenite but segregate at austenite grain boundaries. The segregation of niobium atoms at austenite grain boundaries has been observed through atom probe tomography (APT) in investigations [33, 34], which stabilises austenite grain boundaries and reduces their boundary energy [35].

4.1.2 Transformed from deformed austenite

Differently, subjected to an austenite deformation below T_{nr} , the transformed microstructures cooled at 0.5°C/s and 1°C/s consist of finer PF/QF grains. The BF packets shown in Figure 3a~b disappear in Figure 4a~b. The PF/QF grain refinement and the disappearance of BF packets after austenite deformation can be explained as follows.

Firstly, austenite deformation increases the stored strain energy in austenite. During reconstructive transformations (PF/QF) under slow cooling rates, this strain energy can add to the driving force and make the decomposition of austenite begin at a higher temperature. Therefore, the low-temperature transformation product BF, disappears during the continuous cooling after austenite deformation.

Secondly, austenite deformation can increase the austenite grain boundary area per unit volume and introduce deformation substructures within austenite grains, such as deformation bands or cell boundaries which can act as intragranular nucleation sites [36]. The increase of ferrite nucleation site density accelerates the ferrite transformation kinetics and refines the ferrite grain size. Therefore, the PF/QF grains become finer after austenite deformation. Another effect of austenite deformation is that the increased austenite grain boundaries and deformation substructures are also attractive to the nucleation of niobium carbides, leading to lowered niobium segregation levels at these defects. Therefore, the grain boundary stabilisation effect of niobium atoms is weakened, which reduces the volume fraction of low-temperature transformation products.

Last but not least, strain-induced precipitation of niobium carbide or carbonitride

during austenite deformation below the T_{nr} reduces the niobium content in solution and thus weakens the austenite grain boundary stabilisation effect of niobium.

Therefore, the effect of austenite deformation on the transformation at slow cooling rates can be explained in terms of increasing driving forces, raising nucleation site densities and weakening the effect of niobium in solution on the steel's hardenability.

4.2 Transformed microstructures at high cooling rates

At higher cooling rates ($5\sim 50^\circ\text{C/s}$), the transformed microstructures are either BF or AF dominant and they both are displacive transformation products [28, 37, 38]. As lath boundaries are not necessarily HAGBs for displacive transformation products, the effective grain size refinement should be analysed from two aspects, the density of lath boundaries and the fraction of HAGBs. A high density of lath boundaries and a high fraction of HAGBs means a high density of HAGBs and a small effective grain size. The effective grain sizes of the microstructures transformed from *recrystallized* and *deformed* austenite are discussed separately.

4.2.1 Transformed from recrystallized austenite

From *recrystallized* austenite, the transformed microstructures cooled at $5\sim 50^\circ\text{C/s}$ mainly consist of BF (Figure 3). As the cooling rate is increased, the effective grain size decreases gradually (Figure 7) and the distribution of both HAGBs and LAGBs are changed (Figure 5). These changes in grain refinement and the distribution of HAGBs and LAGBs can be explained from the point of view of variant selection.

As one kind of displacive transformations, BF transformation cannot cross austenite grain boundaries, and BF laths and their parent austenite grains are crystallographically related by an orientation relationship (OR) [2]. Owing to this OR and the symmetry of austenite, there are 24 possible BF orientation variants for each

austenite grain. During BF transformation, some or all of the variants are formed in an austenite grain, and the selection of variants during transformation has a profound influence on the morphology and grain refinement of the final microstructure.

In this research, although the differences of BF microstructures with cooling rates between 5°C/s to 20°C/s are very small, these BF microstructures are quite different from the one cooled at 50°C/s . Therefore, to further investigate the differences in grain refinement from a crystallographic perspective, a comparison is made between BF microstructures cooled at 5°C/s and 50°C/s . A prior-austenite grain was identified in each EBSD maps of these two BF microstructures. The $\{100\}$ pole figures of the BF orientations of these two prior-austenite grains are shown in Figure 8a and c, and the IPF coloured orientation maps of them are illustrated in Figure 9a and d, respectively.

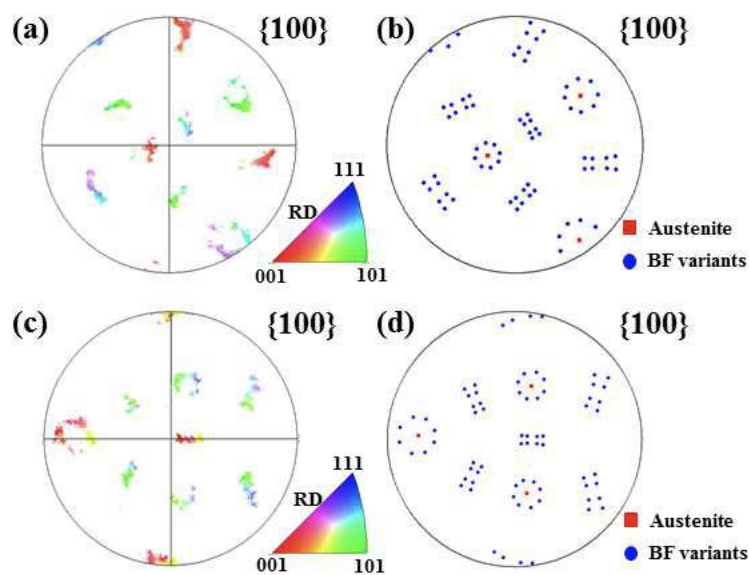


Figure 8 $\{100\}$ pole figures of the BF orientations in single parent recrystallised austenite grains with cooling rates of (a) 5°C/s and (c) 50°C/s ; $\{100\}$ pole figures of the calculated austenite orientations and corresponding BF orientation variants with cooling rates of (b) 5°C/s and (d) 50°C/s , respectively.

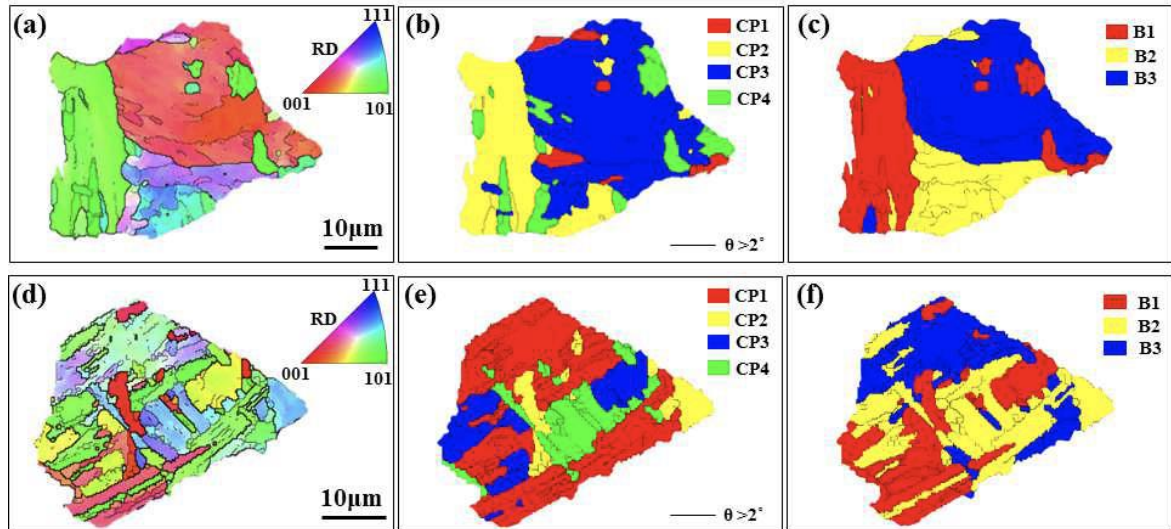


Figure 9 IPF coloured orientation maps (a) and (d), close-packed plane group maps (b) and (e) and Bain group maps (c) and (f) for BF microstructures in single parent recrystallised austenite grains with cooling rates of 5°C/s and 50°C/s, respectively.

To analyse variant selection, the choice of orientation relationship (OR) is critical, as it determines the accuracy of the parent austenite orientation calculation. Although for displacive transformations, various ORs have been proposed, using the OR determined from the inherited phases (e.g. martensite or bainite) increases the accuracy [39]. The method proposed in the study [40] based on boundary misorientations, was used to determine the OR between BF and austenite in this study. ORs are presented as the rotations between FCC and BCC in the form of Bunge Euler angles as shown in Table 2. The angular deviations between close-packed planes (ΔCP) and close-packed directions (ΔCD) of austenite and BF are also listed in Table 2.

Table 2 OR and angular deviations of CP and CD between BCC and FCC

Cooling Rates (°C/s)	Orientation Relationship (°)			ΔCD (°)	ΔCP (°)
5	113.236	8.122	22.8952	2.5176	2.4881
10	114.002	8.07593	22.1349	2.6148	2.4555
20	113.346	8.11413	22.7846	2.5331	2.4847
50	117.657	8.6182	18.7086	2.5265	1.68

It can be found that the change of ΔCD between different microstructures is very small and the ΔCP of microstructures cooled at 5~20°C/s are very close. However, for the microstructure cooled at 50°C/s, its ΔCP is significantly smaller than for the others. This matches the results revealed in the study [41] that the angular deviation between CPs of austenite and BF increases with transformation temperature, while the change in the angular deviation between CDs is small. The temperature dependence of plastic accommodation of the transformation strain in austenite was considered to be the reason behind this [41]. Based on that, the close ΔCP of the microstructures cooled at 5~20°C/s suggests that the transformation temperatures for these microstructures are very close, which of course leads to similar microstructures (Figure 5) and effective grain sizes (Figure 7). In contrast, the smaller ΔCP for the microstructures cooled at 50°C/s indicates that its transformation temperature is evidently lower than for the others.

The ORs listed in Table 2 for 5°C/s and 50°C/s were adopted in this study and the method proposed by Tari et al. [42] was used to evaluate the orientations of these two parent austenite grains. The 24 BF variants of each austenite grain were also calculated. These results are shown in Figure 8 b and d, respectively, and good matches can be found between the pole figures of the experimental BF orientations and the calculated BF orientation variants.

The 24 BF variants calculated can be divided into four close-packed plane (CP) groups, each of which consists of six variants sharing the same parallel relationship of close-packed planes with austenite. BF variants can also be discriminated into three Bain groups according to three distinctive variants of the Bain correspondence [24]. The sequence of the 24 variants and their corresponding CP and Bain groups in this investigation were adopted from Takayama et al. [25]. To reveal detailed crystallographic features, the colours in the orientation maps were changed to show different colours for different CP and Bain groups. These maps are termed as CP and Bain group maps and are shown in Figure 9 b and e, and Figure 9 c and f for the two BF microstructures, respectively.

It can be seen clearly from Figure 8 that more intense variant selection occurred at the cooling rate of 5°C/s than at the cooling rate of 50°C/s . Furthermore, the variant arrangements in these two microstructures are also quite different, as shown in Figure 9. At the cooling rate of 5°C/s , variants belonging to the same Bain group are formed adjacent to each other as shown in Figure 9c and those variants that may come from different CP groups are shown in Figure 9b. Differently, at the cooling rate of 50°C/s , variants belonging to the same CP group are formed side by side as shown in Figure 9e and these variants may come from different Bain groups, thus resulting in the typical packet morphology of BF.

These differences in variant selection and variant arrangement are similar to the results shown in the study [41] for bainite transformed at different temperatures. It can be well explained by the influence of transformation driving force and accommodation methods of transformation strain on variant selection. At the low cooling rate of 5°C/s , BF transformation takes place at high temperatures. Owing to the low BF transformation driving forces at high temperatures, intense variant selection occurs and those variants which are more energetically favoured are selected. Moreover, variants belonging to the same Bain group are formed adjacent to each other to reduce the boundary energy between variants [41], as variant pairs from the same Bain group usually have smaller misorientation angles [25].

While at the high cooling rate of 50°C/s , BF transformation occurs at low temperatures, and owing to the large BF transformation driving forces at low temperatures, variant selection is weakened. Moreover, due to the low transformation temperatures, the strength of austenite and BF are relatively high and the BF transformation strain cannot be relaxed easily by plastic accommodation. It needs to be relaxed by self-accommodation through the formation of variants belonging to the same CP group but different Bain group in neighbours, as introduced in the study [43]. Since the boundaries between variants belonging to different Bain groups have misorientation angles higher than 47.1° [25], a higher fraction of HAGBs will be formed at the cooling rate of 50°C/s than at the cooling rate of 5°C/s and some of these HAGBs exist within the BF packets.

To sum up, with the cooling rate increasing from 5°C/s to 50°C/s, BF laths become finer, leading to a higher density of lath boundaries. Meanwhile, a higher fraction of HAGBs were formed at the cooling rate of 50°C/s than at the cooling rate of 5°C/s due to the weakened variant selection and the self-accommodation of transformation strain as illustrated above. All these factors lead to a higher density of HAGBs and thus a smaller effective grain size at higher cooling rates. It is also reasonable to conceive that by further increasing the cooling rate and thus lowering the transformation temperature, the effective grain size will become increasingly small.

4.2.2 Transformed from deformed austenite

From *deformed* austenite, the transformed microstructures are AF dominant at the cooling rates between 5~20°C/s (Figure 4c~e). At the higher cooling rate of 50°C/s, the transformed microstructure becomes BF dominant with a clear parallel morphology (Figure 4f). This change suggests that with the increase of cooling rate, microstructures gradually transition from AF dominant to BF dominant.

The reason for the transition from AF dominant to BF dominant was explored in our previous study [8]. A brief explanation is provided here. AF and BF both are bainitic transformation products, and they are formed under similar thermodynamic conditions [28, 37, 38]. However, the nucleation sites for AF and BF are different, austenite deformation substructures for AF and austenite grain boundaries for BF. Since austenite grain boundaries are more potent nucleation sites, BF laths nucleate firstly during cooling. If these BF laths develop across the whole austenite grain or impinge with other boundary nucleated BF laths, a BF dominant microstructure is formed. On the other hand, if these boundary nucleated BF laths are stifled prematurely and cannot take up the whole parent austenite grain, AF transformation happens during the subsequent cooling process. Therefore, the introduction of intragranular nucleation sites and the suppression of BF laths nucleated firstly on austenite grain boundaries are the two conditions that should be fulfilled for the occurrence of AF transformation. Austenite deformation introduces a high density of dislocations which can act as intragranular nucleation sites for AF. Besides, austenite

deformation substructures can also suppress the lengthening of BF laths through a mechanism called the mechanical stabilisation of austenite. The suppression of BF laths lengthening can only occur under relatively slow cooling rates or high transformation temperatures. This is because a high cooling rate results in a low transformation temperature which increases the driving stress for transformation interfaces to overcome austenite deformation substructures, which finally leads to a BF dominant microstructure [8]. Consequently, AF microstructure can only be formed at relatively slow cooling rates, and the transformed microstructure gradually transitions from AF dominant to BF dominant with the rise of cooling rates.

Accompanying this microstructural transition, the effective grain size firstly is reduced from 3.2 μm to 2.9 μm with the cooling rate increasing from 5°C/s to 10°C/s, and then increased continuously from 2.9 μm to 3.5 μm as the cooling rate is raised from 10°C/s to 50°C/s, Figure 7b.

The effective grain size is refined with the cooling rate changing from 5°C/s to 10°C/s, because the relatively coarse PF/QF grains in Figure 6i are replaced by fine AF laths in Figure 6j. For AF dominant microstructures (5~20°C/s), due to the large density of intragranular nucleation sites and the suppression effect of deformation substructures on the growth of displacive transformation products, both AF and BF laths are greatly refined as shown in Figure 6a~c, compared with the BF microstructures transformed from *recrystallised* austenite in Figure 5a~c. Therefore, AF dominant microstructures have an intrinsic high density of lath boundaries. Furthermore, the introduction of intragranular nucleation sites weakens variant selection and thus more variants and more types of variant arrangements are generated, leading to a high fraction of HAGBs. This is because as illustrated in Section 4.2.1, at relatively slow cooling rates or high transformation temperatures, bainite transformation favours variants belonging to the same Bain group [41], resulting in a low density of HAGBs. While for AF, these laths mainly nucleate at intragranular nucleation sites, namely austenite deformation substructures, instead of sympathetically nucleating for a low boundary energy between variants as in BF. Consequently, AF dominant microstructures usually have a high density of HAGBs

and a small effective grain size.

The rise of effective grain size from 2.9 μm to 3.5 μm with the cooling rate increasing from 10°C/s to 50°C/s can be attributed to the transition from AF to BF. With the increased cooling rates or the lowered transformation temperatures, the fraction of AF is decreased while that of BF is raised as shown in Figure 4d~f. For BF transformation, the main nucleation sites are austenite grain boundaries, and austenite deformation can only result in a very limited increase of austenite grain boundary area. Even worse, austenite deformation can result in a strong BF variant selection that BF variants with their habit planes parallel to the active slip planes during austenite deformation are favoured [44]. This variant selection can be manifested in Figure 4f that the traces of BF lath boundaries on the RD-ND plane are close to 45° away from the RD. Based on a Schmid factor analysis for the main ideal texture component of austenite during plane strain compression [45], the traces of active slip planes in the RD-ND plane are 19.5~45° away from the RD. Therefore, for *deformed* austenite and with the increased cooling rates, due to the raised BF area fraction and the strong BF variant selection, effective grain sizes become increasingly large as shown in Figure 7b. More importantly, by increasing the cooling rates or lowering the transformation temperatures, the fraction of BF can be further increased as illustrated above, and thus the effective grain size will be continuously increased.

Another difference between *deformed* and *recrystallised* austenite is that there are strain-induced precipitates of NbC or Nb(CN) in the *deformed* austenite, which effectively pin the austenite deformation substructures, leaving austenite grains pancaked. After austenite deformation, these precipitates still exist in the steel and their influence on the subsequent fcc to bcc phase transformation could be analysed in terms of nucleation and growth.

As for the influence of precipitate on growth, Ashby [46] proposed that the area occupied by particles on the boundary must be recreated before the boundary moves, which is the energy pinning the boundary and referred to as Zener drag. When the Zener drag is higher or equal to the boundary moving driving force, boundary

movement is prevented [47]. By the strain-induced precipitation of NbC or Nb(CN), boundary movement involved in recrystallization and grain growth could be prevented, due to their relatively low driving force, 2~20MPa and 0.6~0.01MPa for recrystallization and grain growth, respectively [48]. However, for phase transformation in HSLA steels, its driving force could reach 7~35MPa and 42~84MPa for reconstructive and displacive transformations, respectively [49], which is significantly larger than those of recrystallization and grain growth. According to Ashby's research [46], particles with a volume fraction of 20% and a size of 10nm could prevent the phase interface movement with a driving force in orders of 10MPa, which is not likely in microalloyed HSLA steels. Therefore, although NbC and Nb(CN) precipitates are effective in pinning austenite deformation substructures, their influence on phase transformation interface movement is negligible.

As for the influence of precipitate on nucleation, although there have been investigations suggesting that titanium and vanadium bearing precipitates stimulate ferrite nucleation in steels [50, 51], there are few reports on the possible role of NbC and Nb(CN) precipitates. Further research is needed for clarifying the influence of NbC and Nb(CN) precipitates on the nucleation of fcc to bcc phase transformation.

4.3 Cooling rate dependent effective grain refinement

Having analysed the characteristics of the microstructures transformed from both *recrystallised* and *deformed* austenite, the influence of austenite deformation on effective grain size refinement could be understood. The whole cooling rate range may be divided into four regions as illustrated in Figure 10.

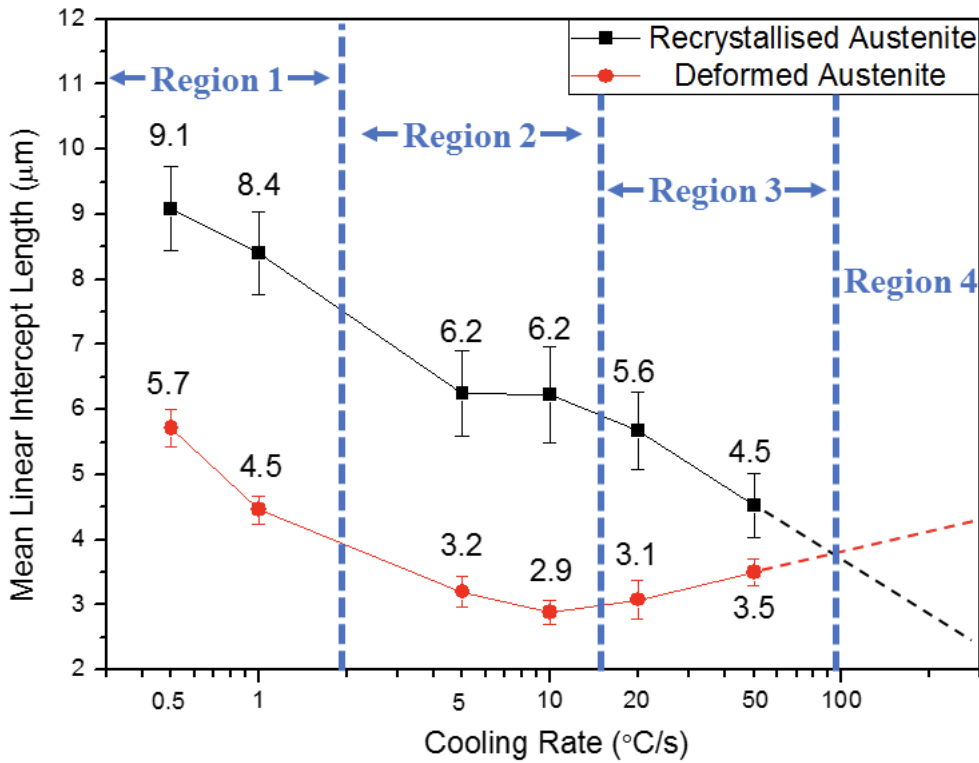


Figure 10 Effective grain size measured as the geometric mean of the linear interception lengths in horizontal and vertical directions from the EBSD maps of the transformed microstructures, where error bars represent 95% confidence levels of the measurement.

In region 1, as described in Section 4.1, due to the low cooling rates (0.5°C/s and 1°C/s), the transformation products consist of PF/QF and BF (from *recrystallised* austenite) or PF/QF and microphases (from *deformed* austenite). Because of the increase in driving force, the rise of nucleation site density and the weakening of the effect of niobium on hardenability, the effective grain size is refined by austenite deformation under these conditions.

In region 2, the transformed microstructures are BF (from *recrystallised* austenite) or AF dominant (from *deformed* austenite). As introduced in Section 4.2.1, BF transformed at relatively slow cooling rates or high transformation temperatures has a low density of lath boundaries and favours variants belonging to the same Bain group

[41], resulting in a low density of HAGBs. In contrast, AF dominant microstructures have an intrinsic high density of lath boundaries and the intragranular nucleation characteristic of AF weakens variant selection, finally leading to a high density of HAGBs. Consequently, the effective grain size is also refined by austenite deformation in this region.

In region 3, although it is evident that the effective grain size is refined by austenite deformation, the developing trends of effective grain sizes with the rise of cooling rate are very different for *recrystallised* and *deformed* austenite. For *recrystallised* austenite, a higher density of lath boundaries and a higher fraction of HAGBs are formed with the rise of the cooling rate as illustrated in Section 4.2.1, leading to a higher density of HAGBs and thus a smaller effective grain size at higher cooling rates. Based on that, it is reasonable to deduct that by further increasing the cooling rate, the effective grain size will become increasingly small. In contrast, for *deformed* austenite, due to the transition from AF to BF and the strong BF variant selection explained in Section 4.2.2, the effective grain size becomes increasingly large with the rise of cooling rate. It is conceivable that by further raising the cooling rate, the fraction of BF will be increased, and thus the effective grain size will be continuously increased. Another aspect needed to be addressed is that the transformation temperature for deformed austenite is higher than for recrystallized austenite at the same cooling rate, and, thus, if the microstructures are the BF dominant in both cases, the temperature-dependent variant selection in BF as illustrated in Section 4.2.1, will result in a decreased fraction of HAGBs for deformed austenite.

According to the developing trends and explanations given above, it is reasonable to conceive that the two solid lines in Figure 10 may intersect at a certain cooling rate higher than 50°C/s, and further increasing the cooling rates, the red line will be above the black line. This suggests that at very high cooling rates region 4 may exist. In this region, instead of refining, austenite deformation will lead to a larger effective grain size. This conception has been confirmed in investigation [52] that at cooling rates higher than 20°C/s, the effective grain size is increased by austenite deformation. The smaller intersecting cooling rate, 20°C/s, in investigation [52] may be attributed to the large hardenability of the steel used in that research because of its large austenite grain size, 125µm.

Based on the analysis above, the controversial effect of austenite deformation on effective grain size refinement can be well understood as being cooling rate dependent. In investigations [10, 16, 17], due to the high transformation temperatures or the low cooling rates, the transformed microstructures from *deformed* austenite are PF/QF or AF dominant so that the transformed microstructures are refined by austenite deformation as in regions 1~3 in Figure 10. However, in investigations [11, 18-20], owing to the high cooling rates (50°C/s [11, 18]) or the low transformation temperatures (350°C [19], 400°C [20]), BF microstructure dominated, therefore, the transformed microstructures are coarsened by austenite deformation as in region 4 in Figure 10.

5 Conclusion

In this study, a low carbon Nb microalloyed steel was subjected to different austenite deformation conditions and was continuously cooled at a wide range of cooling rates (0.5~50°C/s) to investigate the influence of austenite deformation on effective grain size refinement. It was found that:

- (1) At low cooling rates of 0.5~1°C/s, the transformed microstructures consist of PF/QF grains plus BF packets for recrystallised austenite, and PF/QF grains plus microphases for deformed austenite. Because of the increase of driving force, the rise of nucleation site density and the weakening of the effect of niobium on hardenability, the effective grain size is refined by austenite deformation at these cooling rates.
- (2) At cooling rates of 5~10°C/s, the transformed microstructures are BF (recrystallised austenite) or AF dominant (deformed austenite). At these cooling rates, BF microstructures have a low density of lath boundaries and favour variants belonging to the same Bain group, resulting in large effective grain sizes. In contrast, AF dominant microstructures have an intrinsic high density of lath boundaries and weakened variant selection as a result of intragranular nucleation. Consequently, the effective grain size is refined by austenite deformation under these conditions.
- (3) At cooling rates of 20~50°C/s, although the effective grain size is refined by austenite deformation, the developing trends with the rise of cooling rate are very different, decreasing for recrystallised austenite while increasing for deformed austenite. The transition from AF to BF and the strong BF variant selection were proposed to be responsible for the increased effective grain

size for deformed austenite.

- (4) According to the experimental results, the influence of austenite deformation on effective grain size was proposed to be cooling rate dependent in a wider cooling rate range, and possible explanations for the contradicting results in the literature were discussed based on this.

Acknowledgements

This work was supported by the Companhia Brasileira de Metalurgia e Mineração (CBMM), the Hebei Province Overseas Scholar Funding Project [C201817] and the Hebei Province Natural Science Foundation - Iron and Steel Joint Research Foundation [E2019318013].

Reference

- [1] H. Kitahara, R. Ueji, N. Tsuji, Y. Minamino, Crystallographic features of lath martensite in low-carbon steel, *Acta Mater* 54 (2006) 1279-1288.
- [2] S. Kim, Y. Kim, Y. Lim, N.J. Kim, Relationship between yield ratio and the material constants of the Swift equation, *Met Mater-int* 12 (2006) 131-135.
- [3] A.-F. Gourgues, Electron backscatter diffraction and cracking, *Mater Sci Tech* 18 (2002) 119-133.
- [4] L. Fan, D. Zhou, T. Wang, S. Li, Q. Wang, Tensile properties of an acicular ferrite and martensite/austenite constituent steel with varying cooling rates, *Mater Sci Eng A* 590 (2014) 224-231.
- [5] N. Isasti, D. Jorge-Badiola, M.L. Taheri, P. Uranga, Phase transformation study in Nb-Mo microalloyed steels using dilatometry and EBSD quantification, *Metall Mater Trans A* 44 (2013) 3552-3563.
- [6] F.R. Xiao, B. Liao, Y.Y. Shan, G.Y. Qiao, Y. Zhong, C. Zhang, K. Yang, Challenge of mechanical properties of an acicular ferrite pipeline steel, *Mater Sci Eng A* 431 (2006) 41-52.
- [7] D. Bai, S. Yue, T. Maccagno, J. Jonas, Effect of deformation and cooling rate on the microstructures of low carbon Nb-B steels, *ISIJ Int* 38 (1998) 371-379.
- [8] H. Zhao, B.P. Wynne, E.J. Palmiere, Conditions for the occurrence of acicular ferrite transformation in HSLA steels, *J Mater Sci* 53 (2018) 3785-3804.
- [9] H. Zhao, E.J. Palmiere, Effect of austenite grain size on acicular ferrite transformation in a HSLA steel, *Mater Charact* 145 (2018) 479-489.
- [10] H. Zhao, E.J. Palmiere, Effect of Austenite Deformation on the Microstructure Evolution and Grain Refinement Under Accelerated Cooling Conditions, *Metall Mater Trans A* 48 (2017) 3389-3399.
- [11] N.Y. Zolotarevskii, A. Zisman, S. Panpurin, Y.F. Titovets, S. Golosienko, E. Khlusova, Effect of the Grain Size and Deformation Substructure of Austenite on the Crystal Geometry of Bainite and Martensite in Low-Carbon Steels, *Met Sci Heat Treat* 55 (2014) 550-558.
- [12] E.J. Palmiere, C. Garcia, A. DeArdo, The influence of niobium supersaturation in austenite on the static recrystallization behavior of low carbon microalloyed steels, *Metall Mater Trans A* 27 (1996)

951-960.

- [13] T. Kvackaj, I. Mamuzic, A quantitative characterization of austenite microstructure after deformation in nonrecrystallization region and its influence on ferrite microstructure after transformation, *ISIJ Int* 38 (1998) 1270-1276.
- [14] R. Zhang, J. Boyd, Bainite transformation in deformed austenite, *Metall Mater Trans A* 41 (2010) 1448-1459.
- [15] H.K.D.H. Bhadeshia, *Bainite in steels*, Institute of Materials, London, 1992.
- [16] J.H. Beynon, C.M. Sellars: High Strength Low Alloy Steels Conf., Wollongong, 1984, TMS, Warrendale, PA, 1984, pp. 142-50.
- [17] M. Olasolo, P. Uranga, J.M. Rodriguez-Ibabe, B. López, Effect of austenite microstructure and cooling rate on transformation characteristics in a low carbon Nb-V microalloyed steel, *Mater Sci Eng A* 528 (2011) 2559-2569.
- [18] S. Panpurin, N.Y. Zolotarevsky, Y.F. Titovets, A. Zisman, E. Khlusova, Crystallographic features of low-carbon bainite formed under non-isothermal conditions, *Mater Sci Forum*, 762 (2013) 110-115.
- [19] H. Kawata, K. Sakamoto, T. Moritani, S. Morito, T. Furuhashi, T. Maki, Crystallography of ausformed upper bainite structure in Fe-9Ni-C alloys, *Mater Sci Eng A* 438 (2006) 140-144.
- [20] L. Malet, M. Barnett, P. Jacques, S. Godet, Variant selection during the γ -to- α phase transformation in hot-rolled bainitic TRIP-aided steels, *Scripta Mater* 61 (2009) 520-523.
- [21] T. Araki, *Atlas for bainitic microstructures*, ISIJ, Tokyo, Japan, 1992.
- [22] G. Krauss, S.W. Thompson, Ferritic microstructures in continuously cooled low-and ultralow-carbon steels, *ISIJ Int* 35 (1995) 937-945.
- [23] E. Wilson, The γ -to- α transformation in low carbon irons, *ISIJ Int* 34 (1994) 615-630.
- [24] D. Tian, L.P. Karjalainen, B. Qian, X. Chen, Correlation between microstructural features of granular bainite, roughness of fracture surface and toughness of simulated CGHAZ in QT type HSLA steels, *Scand J Metall* 25 (1996) 87-94.
- [25] H.J. Jun, J. Kang, D. Seo, K. Kang, C. Park, Effects of deformation and boron on microstructure and continuous cooling transformation in low carbon HSLA steels, *Mater Sci Eng A* 422 (2006) 157-162.
- [26] Y. Smith, A. Coldren, R. Cryderman, *Manganese-Molybdenum-Niobium Acicular Ferrite Steels with High Strength and Toughness, Toward improved ductility and toughness*, Climax Molybdenum Company (Japan) Ltd, Kyoto, 1972, pp. 119-142.
- [27] Y. Zhong, F. Xiao, J. Zhang, Y. Shan, W. Wang, K. Yang, In situ TEM study of the effect of M/A films at grain boundaries on crack propagation in an ultra-fine acicular ferrite pipeline steel, *Acta Mater* 54 (2006) 435-443.
- [28] Y.M. Kim, H. Lee, N.J. Kim, Transformation behavior and microstructural characteristics of acicular ferrite in linepipe steels, *Mater Sci Eng A* 478 (2008) 361-370.
- [29] G. Rees, J. Perdrix, T. Maurickx, H. Bhadeshia, The effect of niobium in solid solution on the transformation kinetics of bainite, *Mater Sci Eng A* 194 (1995) 179-186.
- [30] M. Thomas, G. Michal, The Influence of Niobium and Nb (C, N) Precipitation on the Formation of Proeutectic Ferrite in Low-Alloy Steels, in: H.I. Aaronson (Ed.) *Solid to Solid Phase Transformations*, TMS-AIME, Warrendale, PA, 1981, pp. 469-473.
- [31] M. Enomoto, N. Nojiri, Y. Sato, Effects of vanadium and niobium on the nucleation kinetics of proeutectoid ferrite at austenite grain boundaries in Fe-C and Fe-C-Mn alloys, *Mater T JIM* 35(12) (1994) 859-867.
- [32] K. Hulka, J. Gray, *High Temperature Processing of Line Pipe Steels*, Proceedings of the International Symposium Niobium, 2001, pp. 587-612.
- [33] H. Wang, Z. Tong, J. Wang, P. Hodgson, I. Timokhina, Study of Nb non-equilibrium segregation at prior austenite grain boundary in welding using atom probe tomography and modeling, *J Mater Sci* 54(16) (2019) 11320-11327.

- [34] H. Wang, J. Wang, Z. Tong, P. Hodgson, X. Wan, K. Wu, R. Wei, I. Timokhina, Characterization of Nb Interface Segregation During Welding Thermal Cycle in Microalloyed Steel by Atom Probe Tomography, *Metall Mater Trans A* 49(12) (2018) 6224-6230.
- [35] R.R. de Avelaz, Niobium Technical Report, NbTR, 01/82, CBMM, Brazil, 1982.
- [36] F. Xiao, B. Liao, D. Ren, Y. Shan, K. Yang, Acicular ferritic microstructure of a low-carbon Mn–Mo–Nb microalloyed pipeline steel, *Mater Charact* 54 (2005) 305-314.
- [37] Y.M. Kim, S.Y. Shin, H. Lee, B. Hwang, S. Lee, N.J. Kim, Effects of molybdenum and vanadium addition on tensile and charpy impact properties of API X70 linepipe steels, *Metall Mater Trans A* 38 (2007) 1731-1742.
- [38] Z. Tang, W. Stumpf, The role of molybdenum additions and prior deformation on acicular ferrite formation in microalloyed Nb–Ti low-carbon line-pipe steels, *Mater Charact* 59 (2008) 717-728.
- [39] G. Miyamoto, N. Iwata, N. Takayama, T. Furuhashi, Mapping the parent austenite orientation reconstructed from the orientation of martensite by EBSD and its application to ausformed martensite, *Acta Mater* 58 (2010) 6393-6403.
- [40] N.Y. Zolotarevsky, S. Panpurin, A. Zisman, S. Petrov, Effect of ausforming and cooling condition on the orientation relationship in martensite and bainite of low carbon steels, *Mater Charact* 107 (2015) 278-282.
- [41] N. Takayama, G. Miyamoto, T. Furuhashi, Effects of transformation temperature on variant pairing of bainitic ferrite in low carbon steel, *Acta Mater* 60 (2012) 2387-2396.
- [42] V. Tari, A. Rollett, H. Beladi, Back calculation of parent austenite orientation using a clustering approach, *J Appl Crystallogr* 46 (2013) 210-215.
- [43] S. Morito, H. Tanaka, R. Konishi, T. Furuhashi, T. Maki, The morphology and crystallography of lath martensite in Fe-C alloys, *Acta Mater* 51 (2003) 1789-1799.
- [44] G. Miyamoto, N. Iwata, N. Takayama, T. Furuhashi, Variant selection of lath martensite and bainite transformation in low carbon steel by ausforming, *J Alloy Compd* 577 (2013) S528-S532.
- [45] A.S. Taylor, P. Cizek, P.D. Hodgson, Orientation dependence of the substructure characteristics in a Ni–30Fe austenitic model alloy deformed in hot plane strain compression, *Acta Mater* 60(4) (2012) 1548-1569.
- [46] M. Ashby, The influence of particles on boundary mobility, *Recrystallization and Grain Growth of Multi-Phase and Particle-Containing Materials* (1980) 325-336.
- [47] S. Subramanian, M. Xiaoping, K. Rehman, Austenite grain size control in upstream processing of niobium microalloyed steels by nano-scale precipitate engineering of TiN-NbC composite, *Energy Materials 2014*, Springer2014, pp. 639-650.
- [48] F.J. Humphreys, M. Hatherly, *Recrystallization and related annealing phenomena*, Elsevier2012.
- [49] L. Sun, The effects of strain path reversal on austenite grain subdivision, recrystallisation and phase transformations in microalloyed steel, University of Sheffield, 2012.
- [50] M. Linaza, J. Romero, J. Rodriguez-Ibabe, J. Urcola, Improvement of fracture toughness of forging steels microalloyed with titanium by accelerated cooling after hot working, *Scripta Metallurgica et Materialia;(United States)* 29(9) (1993).
- [51] K. He, D. Edmonds, Formation of acicular ferrite and influence of vanadium alloying, *Mater Sci Tech* 18(3) (2002) 289-296.
- [52] N. Isasti, D. Jorge-Badiola, M. Taheri, B. López, P. Uranga, Effect of Composition and Deformation on Coarse-Grained Austenite Transformation in Nb-Mo Microalloyed Steels, *Metall Mater Trans A* 42(12) (2011) 3729-3742.